Exp Fluids (2010) 49:911–923
DOI 10.1007/s00348-010-0883-3

RESEARCH ARTICLE

Ballistic imaging in the near-field of an effervescent spray

Mark Linne · David Sedarsky · Terrence Meyer · James Gord · Campbell Carter

Received: 3 January 2010 / Revised: 1 April 2010 / Accepted: 12 April 2010 / Published online: 29 April 2010

Abstract We have investigated liquid breakup mechanisms in the near nozzle region of a high-pressure effervescent atomizer using ballistic imaging. This technique has revealed various breakup regimes depending upon total flow rate and the gas-to-liquid ratio (GLR). At low total speeds, the jet does not exhibit the wide spread angle and rapid breakup for which effervescent sprays are known, even at high GLR. Above a distinct threshold value for total flow rate, the jet passes through several recognizable flow regimes depending on GLR and it does achieve the expected wide spread angle and rapid breakup. Intermediate GLR's produce interesting flow patterns that seem to be generated by surging at the nozzle exit, and this surging can probably be attributed to the flow pattern just at the nozzle exit. Indeed, specific interior flows seem to generate the most rapid breakup and should be investigated further.

M. Linne (✉)
Division of Combustion, Department of Applied Mechanics, Chalmers University, Gothenburg, Sweden
e-mail: mark.linne@chalmers.se

D. Sedarsky
Combustion Physics, Lund University, Lund, Sweden

T. Meyer
Department of Mechanical Engineering, Iowa State University, Ames, IA, USA

J. Gord · C. Carter
Air Force Research Lab, Wright-Patterson Air Force Base, Dayton, OH, USA

1 Introduction

Pure liquid fuel jets issuing into a cross-flow of air are commonly used in gas turbine combustor ducts or in augmentors. They are simple to use and perform reliably. Even these devices could improve, however, if the liquid could be dispersed and vaporized more rapidly and more controllably. This issue is of much higher importance for a liquid-fueled scramjet. Given the short residence time in the combustor of such an engine, the fuel must be dispersed very quickly. This is not an easy task, and in most cases scramjet experiments have been conducted with hydrogen instead of a liquid fuel. While hydrogen has a very high heat of reaction per unit mass and very high flame speed, it is difficult to store in sufficient amounts to fuel a light-weight scramjet powered aircraft. Liquid aircraft fuels contain fairly high energy per unit mass and they are much easier to store and transport. It is therefore useful to investigate ways to disperse these liquids into such high-speed combustion flows.

Effervescent atomization offers the opportunity to mix liquid fuels very rapidly into a cross-flow of air, producing small droplets that can vaporize quickly, using relatively low injection pressure and fairly large-diameter nozzles (Lefebvre et al. 1988; Sovani et al. 2001). These last two points simplify the combustor design and improve reliability. Effervescent atomization is different from other twin-phase techniques such as air blast atomization because it is not necessary to provide high-speed air (at high pressure). Instead, the gas is mixed into the liquid before it exits into the combustor duct, so the gas pressure inside the injector is slightly higher than the fuel pressure (to ensure that gas bubbles mix into the liquid) and the velocity of the incoming gas can be low.

In most cases (Lefebvre et al. 1988; Sovani et al. 2001, 2005), the gas is introduced into the liquid through a

number of holes passing through the wall separating the two flows, or through a sintered material. Often the gas chamber surrounds the liquid flow and the gas is injected through the walls of the passage into the liquid, or in some cases gas is on the inside with liquid on the outside. Past the point of mixing, the flow inside the nozzle passage is characterized by several regimes delineated primarily by the gas-to-liquid mass ratio (GLR). For low GLR (typically between 0.01 and 0.2), the gas produces dispersed bubbles in the confined liquid (called "bubble-flow"). At somewhat higher GLR (typically around 0.2 and above), the bubbles join to form long cylindrical shapes (called "slug-flow", see the simple representation in Fig. 1). These formations occupy the center of the flow while the liquid flows primarily along the walls of the injector tube, aside from the disk-shaped liquid formations that bridge across and separate the various gas "slugs" from each other. As GLR increases, these slugs quickly merge to form a continuous column of gas which is surrounded by an annulus of liquid (called the "annular-flow regime"). The values for GLR provided here to delineate the various internal flow regimes are simply guidelines. The actual values for GLR at boundaries between regimes depend upon the specific nozzle design.

The effectiveness of this technique is attributed to the fact that the speed of sound in a twin-phase flow is orders of magnitude slower than the same speed in either of the pure substances (Sovani et al. 2001). The flow can thus choke at relatively low velocities, even with relatively large exit orifices (order of several hundred microns up to a millimeter). The change of pressure going from inside to outside of the injector body then causes the bubbles to expand rapidly just as they exit, exerting a force on the liquid structures and very rapidly shattering the liquid column. Especially in the bubble-flow regime this can be a complex, stochastic process that is not easily described in terms of correlations or numerical models. Even in the annular-flow regime it is difficult to estimate velocities, or the bulk properties of the flow (e.g., the speed of sound) with any accuracy.

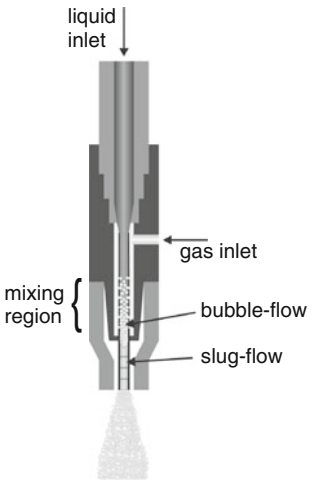

Fig. 1 Schematic of the effervescent nozzle studied here. Liquid flows down the inside passage while gas flows in the outside annulus to the mixing region where holes are drilled in the wall of the liquid tube. The gas bubbles into the liquid in the mixing region. Depending on the gas-to-liquid ratio (GLR) the interior flow can be simply bubbly, it can enter the "slug flow regime" (as depicted), or at higher GLRs it forms an annular regime where an uninterrupted central column of gas is surrounded by an annulus of liquid

Sovani et al. (2001) provide a comprehensive review of work on effervescent sprays up to 2001. Their summary includes the following important general findings: studies of the internal flow confirm the description of the three flow regimes just given; good atomization can be achieved at relatively low injection pressures; at specific injection pressures, effervescent sprays produce smaller droplets than more conventional sprays; the mean drop size is relatively insensitive to viscosity but a strong function of the GLR; the required gas flow rates are much less than those used in other twin-phase spray systems; relatively large exit orifice diameters can be used; if air is used as the aerating gas then air inside the spray core can enhance combustion and produce lower soot levels; the flow velocity at the nozzle exit is usually much lower than conventional atomizers as it chokes at much lower speeds; and effervescent sprays produce much wider cone angles (by up to a factor of 2) than conventional sprays. Conventional spray breakup is affected fairly strongly by the pressure of the gas into which the liquid is injected. Here, the main effect of gas pressure has to do with the difference in pressure experienced by the bubbles as they exit the nozzle. In a general sense, higher pressure differences produce more rapid breakup together with smaller primary droplets. Chamber gas density has a well-known effect on secondary breakup as well, increasing the droplet breakup rate with density. Air entrainment is perhaps the most critical performance metric for effective combustion. In an effervescent spray, entrainment increases with mass flow rate and with GLR. GLR thus provides a potential control actuation. The obvious drawback to effervescent atomization is the need for a compressed gas system. Finally, reference to flow instability and "surging" of effervescent sprays can be found throughout the literature. While this brief review implies general agreement, there are actually some notable disagreements on these topics. They can usually be attributed to differences in the injector designs themselves or extremes of operational regimes.

Since 2001, most of the work on effervescent sprays has focused on specific architectures like diesel injectors (Sovani et al. 2005) and the spray studied here (Lee et al. 2009; Lin et al. 2008, 2009; Sallam et al. 2004) for example. While the droplet field for these sprays has been

well characterized as a function of GLR and other parameters, "more fundamental investigation into the liquid breakup mechanism in the near nozzle region of a high-pressure effervescent atomizer is essential" (Sovani et al. 2001).

2 The effervescent spray under study

The nozzle used in this work and in other closely related projects (Lee et al. 2009; Lin et al. 2008, 2009; Sallam et al. 2006) is depicted in Fig. 1. The liquid flows down the 1.3 mm (0.05 inch) i.d. center tube, while gas flows down the outer annulus surrounding the liquid tube. At the mixing region, 178 μm (0.007 inch) holes in the wall of the liquid tube admit the gas into the liquid (the gas is at somewhat higher pressure than the liquid) and the twin-phase flow proceeds to the nozzle outlet. This injector has both 0.5 mm (0.02 inch) and 1 mm (0.04 inch) i.d. nozzle orifices, and the length-to-diameter ratio is 20.

Sallam et al. (2006) observed this spray as it issued into a supersonic crossflow using double-pulse laser shadowgraphy and holography (for droplet size distributions and velocity). Various fluids were studied (water, ethyl alcohol and glycerol) to access a variety of fluid properties, with GLR between 0.02 and 0.10. The injector pressure was between 0.20 and 3.21 MPa and the jet issued into a 1.94 Mach number flow at 0.21 MPa. Despite the wide range of fluid properties investigated in this work, the overall spray properties were fairly constant. The measured droplet sizes fell between 33 and 60 μm (SMD) for all the liquids tested, and the jet characteristic breakup times were fairly constant as well. The cone angle was a clear function of injector pressure, ranging between 60° and 80° (full angle).

Lee et al. (2009) describe the development of a digital holographic instrument for studies of this and similar sprays. They studied breakup in a subsonic wind tunnel with air speeds between 3 and 60 m/s at normal temperatures and pressures (Mach numbers up to 0.18). They injected water and air through the same effervescent injector but focused just on the 1 mm i.d. nozzle. Both the water and aerating air were held to around 1.1 MPa. One set of injector flow rates was chosen; the water flow rate was 145 cm^3/s and aerating gas flow rate was 100 cm^3/s to give a GLR of 8 (probably in the annular flow regime). These authors applied a double-pulse holographic system with digital analysis allowing them to acquire information on drop size distributions as a function of position, drop sphericity, and the velocities of various liquid structures in the flow. They report drop sizes (SMD) on the order of 40–120 μm, which is at the high end for an effervescent spray but not out of the commonly measured size range. This particular spray has moderate optical density and an accessible droplet size distribution, making it a very good candidate for holography. Lee et al. (2009) emphasize the development of a diagnostic in this first paper but they have taken much more data and a paper emphasizing the mechanics of these sprays will be forthcoming.

In an effort to examine the interior flow near the nozzle exit, Lin et al. (2008, 2009) have performed X-ray phase contrast imaging using the Advanced Photon Source (APS) at Argonne National Laboratory. The goal of such work is to ascertain when the near field transitions from a breakup process characterized by the stripping of droplets from large ligaments to a process characterized by an emerging flow that is shattered into droplets directly, without ligaments in evidence. They investigated just a few run conditions, examining the spray in the near field of the nozzle. They present images from the 0.5 mm nozzle at a GLR of 1.41 with a water flow rate of Q_L = 0.53 L/m. They then present an image zoomed in on the spray and successfully visualize individual bubbles undergoing a bursting process.

Here, we describe complementary work aimed at the same question: when does the near field transition to a process wherein the emerging field is shattered directly into droplets, without ligaments in evidence? We have applied a technique called ballistic imaging (Linne et al. 2009; Paciaroni 2004; Paciaroni and Linne 2004) to image the liquid core under a variety of flow conditions. In what follows we briefly describe the technique, describe the specific experiments, and then present and discuss the experimental results.

3 Experimental program

3.1 Ballistic imaging

The ballistic imaging technique has recently been reviewed so the description provided here is fairly short. Further details can be found in Linne et al. (2009) and the references cited therein. In general, ballistic imaging is an extension of Schlieren or shadowgraphy designed to mitigate obscuration caused by multiply-scattered, spatially disorganized light ("spatial noise") in the measurement volume. Here, the goal is to image larger distributed structures (ligaments and large droplets) that lie inside a dense, optically thick cloud of small droplets. When light passes through a highly turbid medium, a small amount of high- quality imaging light exits. It contains the desired image information and it can be used to construct an image of large interior structures. A small number of photons actually pass straight through without scattering. These are termed "ballistic", hence the name. Because they travel the shortest path, they exit first and are located on the centerline of the input beam. Photons exiting the medium that

have experienced multiple scattering events are the most numerous in materials with a high optical depth. Some of these multiply scattered photons travel nearly the same path as the ballistic photons; they exit at almost the same time and they have a narrow solid angle. These can also contribute to a high quality image of what lies inside a turbid medium. The majority of the multiply scattered photons constitute spatial noise, however, that corrupts images. Such photons are scattered into a very large solid angle and exit last.

The minimally disturbed path taken by high-quality imaging light allows it to retain intact image information on structures that may be embedded within the turbid medium. The problem of obtaining a high-resolution image through highly scattering materials is thus a matter of segregating the high-quality imaging light from the dominant spatial noise. This can be done using discrimination methods that make use of the properties of the high-quality light; propagation direction, early exit time, polarization, and coherence can be used for segregation.

Our ballistic imaging system was optimized to provide high-resolution, single-shot images of the liquid core in very dense atomizing sprays using time gating (see Fig. 2). The laser system used here was a Coherent Legend Ti:sapphire regenerative amplifier seeded with a Spectra-Physics Tsunami Ti:sapphire mode-locked laser; this system produces a 1 kHz stream of 80 fs long pulses with energy around 2–2.5 mJ. These pulses allow us to gate the early, high-quality imaging light using a very fast shutter. The shutter consists of an optical Kerr effect (OKE) gate capable of 1.8 *ps* gating times. This is used to select just the leading edge of the transmitted light pulse and reject the late-arriving noise photons. Additionally, the geometry of the OKE gate employed here includes both spatial and polarization filtering to enhance collection of high quality light. The image was then relayed to a Phantom v7.0 camera from Vision Research, Inc. This is a high-speed (up to 4,800 frames per second) CMOS imaging device with an 800 × 600 pixel array.

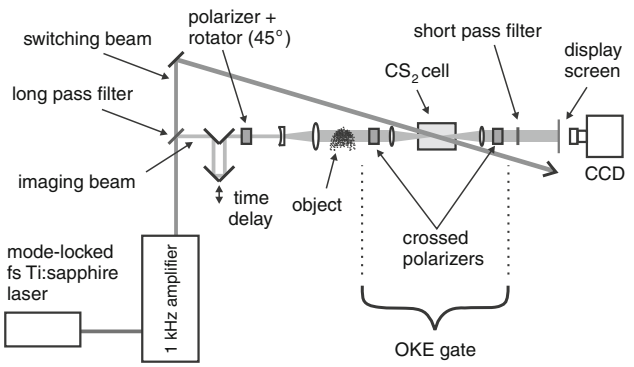

Fig. 2 Schematic of the single-shot, two-band, time-gated ballistic imaging system

Figure 3 contains a representative ballistic image of this spray taken in an earlier campaign (see e.g., Sedarsky et al. 2009). For that work, a Phantom v5.0 camera from Vision Research, Inc. (a CMOS imaging device with an 1,024 × 1,024 pixel array and up to 1,000 frames per second) was used. In Fig. 3, one can see dark regions that represent larger liquid structures and light regions that depict the gas phase. One can also see distinct droplets. Normal white-light shadowgrams of the same flow show just the outer edge of the spray (established by the fine droplet cloud which is not imaged here) and it shows no interior details. It is important to keep in mind that ballistic imaging is also a line of sight technique. The larger, black regions in Fig. 3 are distributed liquid structures (mostly large ligaments) that are thicker than 130 μm. They appear black because it takes light 2 ps longer to cross 130 μm of water than it takes to cross the same distance in air. Any structure with thickness greater than 130 μm will cause a time delay in the refracted light to make it arrive at the OKE gate after it has closed, producing a black image. Note that droplets at the edge of the spray look much more like a normal shadowgram of a droplet, with light and dark regions. Those droplets are smaller than 130 μm, and so a portion of the refracted light makes it through the OKE gate before it shuts.

3.2 Fluid system

In the work described here, the spray depicted in Fig. 1 was supplied with water using a nitrogen-pressurized water reservoir, and the aerating gas was also bottled nitrogen. The separate liquid and gas flows were controlled by a set of choke valves, and continuously measured by a bank of turbine mass flowmeters for the liquid and sonic nozzles for the gas. This arrangement rapidly merged the liquid and gas flows at elevated pressures inside the nozzle, as described earlier. Liquid flow rates used in this work covered the range from 0.17 to 1.1 L/m for the 0.5 mm nozzle and the range from 0.17 to 1.9 L/m

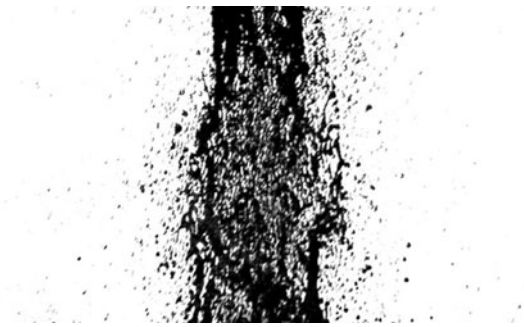

Fig. 3 Ballistic image of an aerated spray with Q_L = 0.67 (L/m) and GLR = 2

for the 1.0 mm nozzle. The nitrogen flow rate was adjusted to provide a GLR from 0.0 to around 8 for both cases. This represents a fairly broad range of flows. After mixing, the two-phase mixture flowed through a convergent connecting volume to a straight nozzle with a circular orifice and a length to diameter ratio of 20. In the work reported here, the spray issued into still air at atmospheric pressure and temperature. This was an appropriate experimental condition because we are investigating the very near field, which is not strongly affected by a cross flow, and effervescent sprays are not generally affected by changes in pressure (especially not the near field).

4 Experimental results

4.1 The 0.5 mm nozzle

The most relevant prior work for this nozzle is the X-ray phase contrast imaging work of Lin et al. (2008, 2009). We have investigated the same flows, together with a range of other flows as just mentioned.

The flow rates used here provide an interesting sequence of images that clearly illustrate the importance of total flow rate through the injector. Much of the prior work on effervescent sprays emphasizes the importance of the GLR. If the water flow rate is held relatively constant, the GLR is indeed the controlling parameter, but total flow rate is perhaps equally important in terms of the breakup mechanics. We therefore present the various run conditions studied here in Table 1 by grouping them into various water flow ranges (Q_L). The water flow rates used for each run were not exactly the same, but the data do break down into three general flow rates. We also calculate a GLR = 0 (water-only) Reynolds number for each of the water flow rate ranges. This is done simply to provide a reference dimensionless number for the various flow rate ranges. It would also be very useful to know the Mach number for each flow when gas is injected, but the uncertainties of such an estimation were judged so large as to render the calculation uninformative. Within each water flow range, the presentation starts from the lowest and goes to the highest GLR.

The images that follow have been extracted from a sequence of images (sometimes up to 50) taken at 1 kHz frame rate. They have been chosen for this publication because they are fairly representative. Having said that, it is important to acknowledge again that effervescent sprays are known to have an unsteadiness that is a function of the flow rates, sometimes reaching the point where they have a characteristic surging. Motion pictures can be used to observe this phenomenon and its effect on breakup.

Table 1 Effervescent spray run conditions for the 0.5 mm nozzle

Case no.	Q_L (L/min)	GLR
$Q_L \sim 0.17$ (L/m), $Q_L/D \sim 0.34$ (L/m–mm), $Re_{water} \sim 9{,}000$		
1	0.18	0.00
2	0.17	1.73
3	0.17	4.66
4	0.17	7.03
$Q_L \sim 0.47$ (L/m), $Q_L/D \sim 0.94$ (L/m–mm), $Re_{water} \sim 25{,}000$		
5	0.47	0.00
6	0.48	2.01
7	0.48	8.00
$Q_L \sim 0.55$ (L/m), $Q_L/D \sim 1.10$ (L/m–mm), $Re_{water} \sim 28{,}000$		
8	0.53	1.43
$Q_L \sim 0.64$ (L/m), $Q_L/D \sim 1.28$ (L/m–mm), $Re_{water} \sim 34{,}000$		
9	0.65	0.00
10	0.64	1.16
11	0.64	2.41
$Q_L = 1.11$ (L/m), $Q_L/D \sim 2.22$ (L/m–mm), $Re_{water} \sim 54{,}000$		
12	1.11	0.00

Interesting, unsteady cases will be identified in the text that follows.

In what follows, the dimensions of each ballistic image are 7 mm per side. The grainy nibs at the top of each image locate the injector tip. They are grainy because the tip was not directly illuminated by the imaging beam. The spatial resolution of these experiments was limited more by the camera used than by the instrument. If one compares Fig. 3 to the figures that are to follow, one can see that point immediately. Figure 3 came from a short-term campaign using a camera with higher spatial resolution; everything else in the setup was identical. For the images presented below, the spatial resolution was likely around 30 μm. This is just an estimate based on former work (Paciaroni and Linne, 2004); we did not measure the system resolution for this specific setup.

First consider Case numbers 1, 5, 9 and 12 (Figs. 4a, 6a, 9a, 11). These all represent GLR = 0 flow cases (for which we calculate the Reynolds numbers, Re_{water}, in Table 1) and their respective images are almost identical. One can see a progression of surface disturbances that start at low *Re* with what appear to be a Rayleigh–Taylor instability, and then as *Re* increases some turbulent wrinkling appears, especially for Case number 12. The progression clearly tracks the *Re*, but this is a fairly large nozzle exit and the images are taken near the nozzle, so the differences are not great.

In Case 2 (Fig. 4b), a low flow of gas has been added to put this jet in the bubble-flow regime. A nearly contiguous liquid core appears near the nozzle, but the expanding bubbles are clearly causing the column to break apart as the

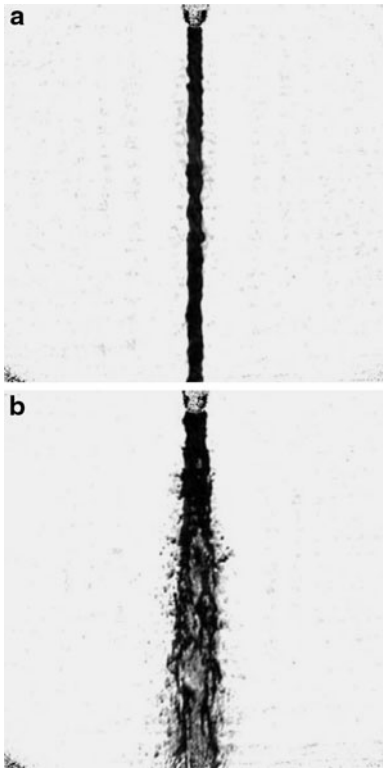

Fig. 4 Ballistic images of flow cases described in Table 1 **a** Case 1: Q_L = 0.18 (L/min), GLR = 0.00; **b** Case 2: Q_L = 0.17 (L/min), GLR = 1.73

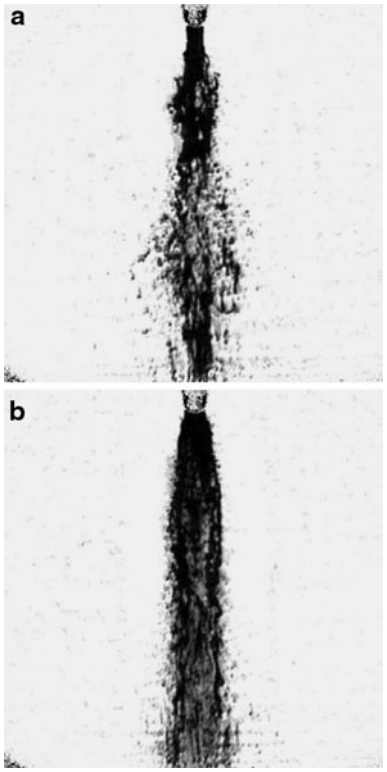

Fig. 5 Ballistic images of flow cases described in Table 1 **a** Case 3: Q_L = 0.17 (L/min), GLR = 4.66; **b** Case 4: Q_L = 0.17 (L/min), GLR = 7.03

mixture flows downward. Large ligaments and drops are in evidence downstream of the liquid column, and the spray flaps weakly over time in a way that is reminiscent of vortex shedding from a gas jet issuing into still air. Case 3 (Fig. 5a) has a GLR that probably places it in the annular-flow regime but the two image sequences (Figs. 4b,5a) are quite similar (although Case 3 exhibits more surging). The spray for Case 3 seems to produce long liquid strands that surround a lighter region. This flow is quite similar to ballistic images of a gas-centered swirl-coaxial injector designed to operate in the annular flow regime (Schmidt et al. 2009). The similarity between Cases 3, 4, and 8 and the work reported in Schmidt et al. (2009) supports the notion that these flows are in the annular flow regime but they are breaking up in a mixed-mode that is not characteristic of most effervescent jets. The gas continues to break the liquid column but the characteristic broadening of the jet that is known to happen with effervescent sprays has not yet occurred. Case 4 has a high GLR and one can clearly see that the center of the liquid column is gas just a few diameters below the nozzle (Fig. 5b). There is little evidence of surging in this case; the jet continues to flap weakly. It is our opinion that the characteristic broadening and rapid breakup of an effervescent jet has not occurred, even at unusually high GLR, because the total flow rates are fairly low. It may be that the flow is not strongly choked at the exit, or that the flow exiting the nozzle is not highly turbulent. These jets break up with a mixed mode similar to the work of Schmidt et al. (2009).

Cases 5–7 use a higher flow rate, and in Figs. 6, 7 one can clearly see a change in the jet behavior. This threshold separating two kinds of breakup mechanics correlates with flow rate throughout our entire dataset; it is caused either by a stronger choke at the nozzle exit or perhaps higher turbulence intensity. Case 6 (Fig. 6b) is probably just entering the slug-flow regime. It used a GLR significantly less than the GLR used in Cases 3 and 4 (Fig. 5a, b), but the jet breaks up much sooner. One can detect ligaments and droplets, but the spray expands rapidly like one would expect of an effervescent jet. This jet flaps like the previous cases (reminiscent of shear layer instabilities like vortex shedding in the surrounding air). Case 7 (Fig. 7a) is quite similar. Both cases 6 and 7 also have evidence for a low frequency, low amplitude surging. Note the faint chevrons of collected droplets downstream. These are difficult to see in the printed images but they are somewhat easier to see enlarged on a computer screen. Figure 7a has been modified in Fig. 7b to emphasize the chevron structure discussed here (contrast was increased by reducing the signal level of the lighter-toned structures). We normally make a point not to manipulate images other

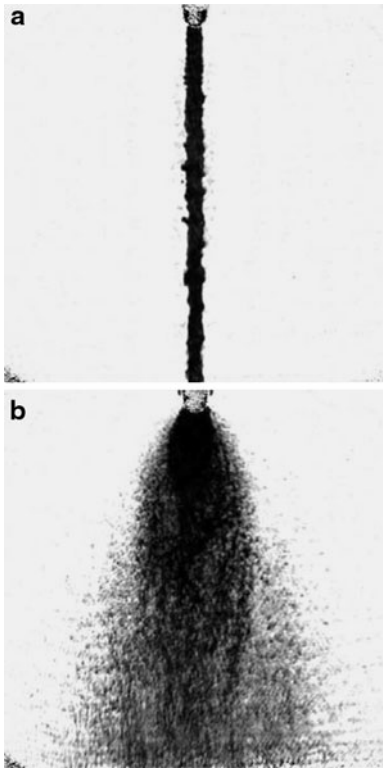

Fig. 6 Ballistic images of flow cases described in Table 1 **a** Case 5: Q_L = 0.47 (L/min), GLR = 0.00; **b** Case 6: Q_L = 0.48 (L/min), GLR = 2.01

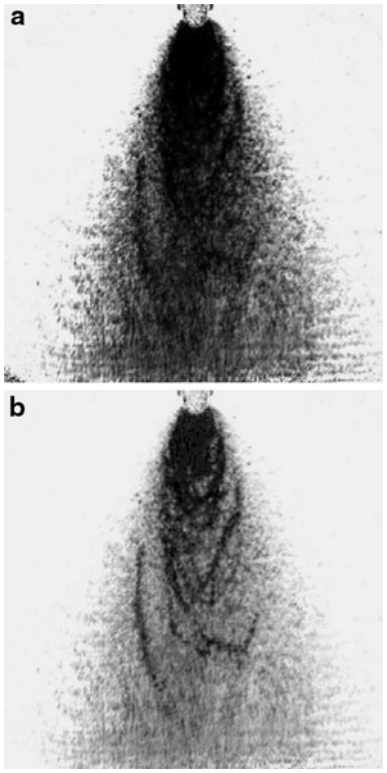

Fig. 7 Ballistic images of flow cases described in Table 1 **a** Case 7: Q_L = 0.48 (L/min), GLR = 8.00; **b** The spray in Case 7 with the background adjusted to call-out the chevron structures that can be found within the flow

than to use normalization and background subtraction, to avoid accidental digital fabrication of information. This is the only image we have modified further, but the modification helps to emphasize the point. These chevron structures are waves produced by the low level surging, which is more obvious in the motion pictures. Each surge bunches droplets into these chevron (wave-like) structures.

Case 8 (Fig. 8) serves two purposes. It serves as the bubble-flow style case for the Case 5–7 sequence, but it also matches the nominal flow settings for Fig. 5b. in Lin et al. (2009). The flow depicted in Fig. 8 is quite different from the figure in Lin et al. (2009); it clearly contains ligaments and it is not broken up as much as Lin and co-workers observed. This disagreement could be caused by difficulty reproducing flow conditions. When Lin and co-workers performed the work described in their paper, they used a flow metering system that was not as accurate as the one that was available for the work reported here. This flow condition is nearing the boundary between the bubble-flow and the slug-flow regimes (as reported in other literature, e.g., Sovani et al. 2001). If Lin et al. (2009) had accidentally wandered into the slug-flow regime, it could explain the difference in observations.

Case 10 is next in the sequence (Fig. 9b). This is for a GLR characteristic of the bubble-flow regime. It compares

Fig. 8 Ballistic image of flow case 8 described in Table 1: Q_L = 0.53 (L/min), GLR = 1.43

well with Case 8 (Fig. 8). Finally, Case 11 (Fig. 10) is probably in the slug-flow regime but at fairly low GLR. It appears to behave in a similar way to the Case 6 and 7 flows (Figs. 6b, 7a).

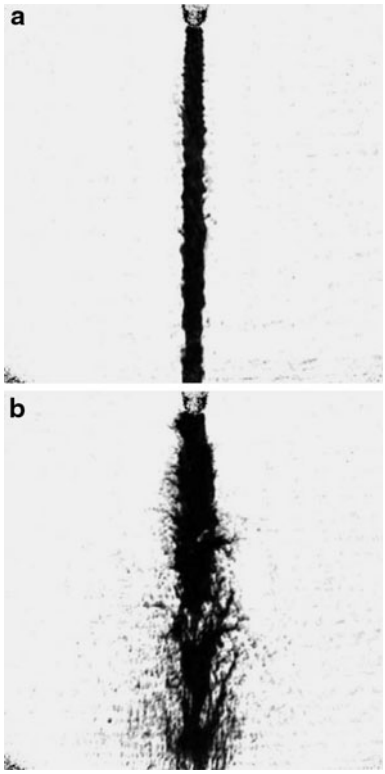

Fig. 9 Ballistic images of flow cases described in Table 1 **a** Case 9: Q_L = 0.65 (L/min), GLR = 0.00; **b** Case 10: Q_L = 0.64 (L/min), GLR = 1.16

Fig. 10 Ballistic images of flow cases described in Table 1 Case 11: Q_L = 0.64 (L/min), GLR = 2.41

4.2 The 1.0 mm nozzle

The most relevant published work on this nozzle was the holographic investigation by Lee et al. (2009), who had the spray issue into a fairly slow, atmospheric pressure cross flow. Their work investigated just one flow and they report droplet sizes and velocities. Here, we investigate a range of flows (as detailed in Table 2) and we focus on the fluid structure of the near field (Fig. 11).

The first two sets of flow cases in Table 2 (Cases 13–20) are similar to the flows in Table 1, but after that they deviate because the larger nozzle produces a somewhat different sequence. As with the 0.5 mm nozzle, the GLR = 0 cases look quite similar to a simple jet issuing into still air.

In Case 14 (Fig. 12b), the air flow should be in the bubble flow regime but it is probably close to a transition to the slug flow regime. A nearly contiguous liquid core appears to be in evidence near the nozzle, but the spray quickly transitions to a weakly surging and flapping flow. The bubbles in the interior are likely joining into larger slugs that then segregate liquid structures. The remaining cases at this water flow rate (cases 15 and 16 in Fig. 13) are similar to the low flow cases for the 0.5 mm nozzle. The jet breaks up into ligaments and large drops via some mixed mode, and it does not exhibit the large spread angle or the rapid breakup of the higher flow rate cases.

Cases 17–20 in Figs. 14, 15 are somewhat different from Cases 5–7 in Figs. 6, 7 (same water flow rate and GLR's), and this is likely caused by the larger orifice; the flow velocity in this set of cases is much less than the velocity of Cases 5–7. The image sequence passes through the phases discussed earlier. The low GLR cases exhibit the mixed mode; they have characteristic ligaments, they flap

Table 2 Effervescent spray run conditions for the 1.0 mm nozzle

Case no.	Q_L (L/min)	GLR
$Q_L \sim$ 0.17 (L/m), Q_L/D $\sim$ 0.17 (L/m–mm), $Re_{water} \sim$ 4,500		
13	0.18	0.00
14	0.18	1.90
15	0.17	4.68
16	0.17	10.02
$Q_L \sim$ 0.47 (L/m), Q_L/D $\sim$ 0.47 (L/m–mm), $Re_{water} \sim$ 12,500		
17	0.47	0.00
18	0.47	2.07
19	0.48	4.16
20	0.47	7.85
$Q_L \sim$ 0.98 (L/m), Q_L/D $\sim$ 0.98 (L/m–mm), $Re_{water} \sim$ 26,000		
21	0.98	0.00
22	0.98	2.15
23	0.98	4.06
24	0.97	8.04
$Q_L \sim$ 1.11 (L/m), Q_L/D $\sim$ 1.11 (L/m–mm), $Re_{water} \sim$ 29,000		
25	1.11	0.00
26	1.11	2.01
27	1.13	4.01
28	1.10	5.98

Fig. 11 Ballistic image of flow case 12 described in Table 1 Q_L = 1.11 (L/min), GLR = 0.00

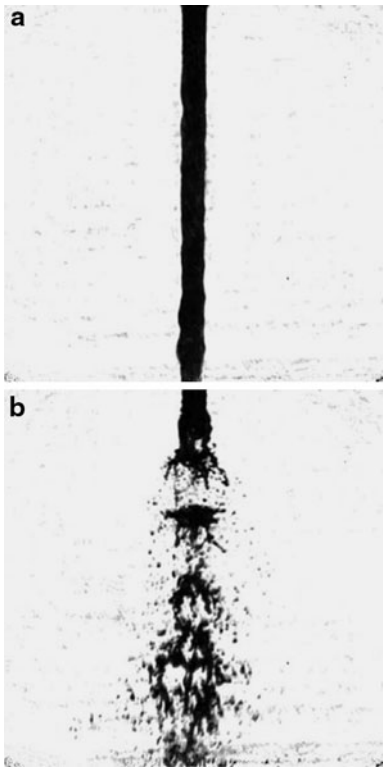

Fig. 12 Ballistic image of flow cases described in Table 2 **a** Case 13: Q_L = 0.18 (L/min), GLR = 0.00; **b** Case 14: Q_L = 0.18 (L/min), GLR = 1.90

weakly and it is not until a high GLR is reached that the jet starts to spread. Case 20 (Fig. 15b) shows a broader spray that is beginning to exhibit weak surging but ligaments are still visible inside the spray. This jet thus crosses from the mixed-mode behavior similar to Cases 1–4, into a rapid

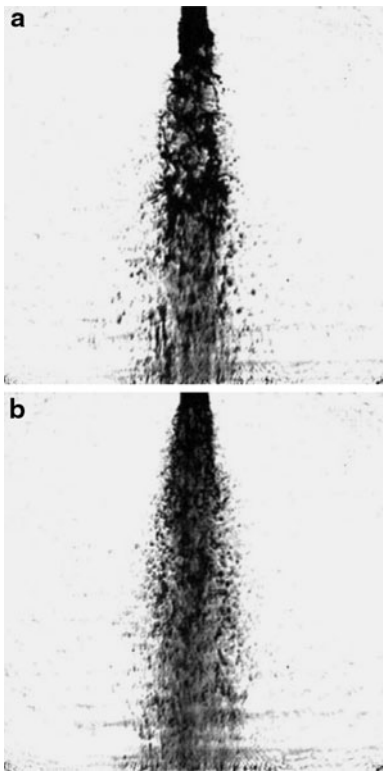

Fig. 13 Ballistic image of flow cases described in Table 2 **a** Case 15: Q_L = 0.17 (L/min), GLR = 4.68; **b** Case 16: Q_L = 0.17 (L/min), GLR = 10.02

breakup mode more characteristic of effervescent sprays. It seems to be right at the threshold.

The next set of flows (Figs. 16, 17) has now transitioned beyond a threshold to produce rapid breakup and characteristically wide jets. Cases 22 and 23 (Figs. 16b, 17a) exhibit characteristic flapping and weak surging. They produce droplet chevrons as a result. Case 24 (Fig. 17b) breaks up even more rapidly producing a more uniform droplet field and a wider spread angle. The circular light and dark pattern on the left hand side of Fig. 17b was caused by diffraction and it is an artifact. It does not image anything related to breakup per se. This case exhibits incoherent flow instability more reminiscent of a shear layer instability. Surging and chevrons were not in evidence. Even when the background manipulation that was applied to Fig. 7b was applied to Fig. 17b, no chevrons could be detected.

The image in Fig. 17b requires some further explanation. The very core of the flow at the nozzle has gone dark even though this technique is meant to image what lies inside. This has happened because the core of the flow has become a field of large droplets. Lee et al. (2009) measured droplets on the order of 40–120 μm for a lower density spray produced by the same nozzle. The spatial resolution of our instrument is on the order of 30 μm, meaning that each of these large droplets can be individually imaged. There are many such

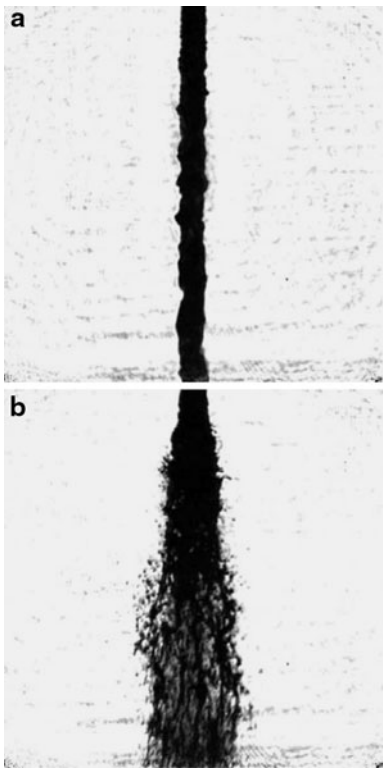

Fig. 14 Ballistic image of flow cases described in Table 2 **a** Case 17: Q_L = 0.47 (L/min), GLR = 0.00; **b** Case 18: Q_L = 0.47 (L/min), GLR = 2.07

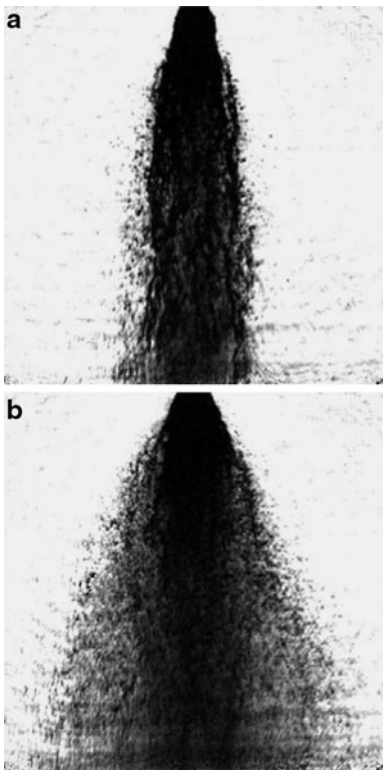

Fig. 15 Ballistic image of flow cases described in Table 2 **a** Case 19: Q_L = 0.48 (L/min), GLR = 4.16; **b** Case 20: Q_L = 0.47 (L/min), GLR = 7.85

drops along the line of sight, they are nearly the same size as the ligaments, and so it becomes impossible to adjust the time delay of the OKE gate to give a transmissive image of the ligaments. We believe that this flow condition will cause a problem with other line-of-sight techniques as well. This dense field of large droplets is too much like a distributed liquid structure along the line of sight. If one considers the images that lead up to this point, one can at least speculate that these darkened, spread images indicate a flow wherein the large ligaments have been replaced by a field of droplets that emerge from the nozzle. This much is clear; these conditions are certainly closer to that goal than any of the others. Perhaps, the best way to resolve this question would be to search for ligaments with structured laser illumination planar imaging (SLIPI, Berrocal et al. 2008), starting at the spray edge and then translating the imaging plane further and further in toward the core until the signal is lost.

Cases 25–28 (Figs. 18, 19) are quite similar to those in Figs. 16, 17. The flow behaviors now follow a regular pattern and increased flows do not introduce new flow physics.

4.3 Observations

The experimental data presented here seem to indicate several trends, for both the 0.5 and the 1.0 mm nozzles. The contributions of this work are in the ballistic images and the motion pictures that accompany them. Unfortunately, we do not have simultaneous images of the flow inside the nozzle, so we rely upon collected observations in the literature (e.g., Sovani et al. 2001). The observations presented in this section are therefore not fully conclusive. More work is required, but we can at least make some speculations about the flow regimes encountered here, to guide further research.

First, at low total flow rates the jet spreading and rapid breakup that is characteristic of effervescent sprays has not been established. There appears to be a total flow rate threshold below which these sprays do not induce rapid breakup. Rather, they exhibit what could be called mixed breakup modes. This behavior could be caused by the failure of the flow to choke at the nozzle or because the value of *Re* is too low. The uncertainty in estimation of the Mach number is too high to establish failure to choke as the cause.

This threshold behavior can in fact be identified in Fig. 20, which presents a plot of Q_L/D vs. GLR for both nozzle diameters of 0.5 and 1.0 mm. Open symbols represent the mixed breakup regimes discussed earlier and solid symbols represent very rapid breakup. In general, there is a progression toward rapid atomization with

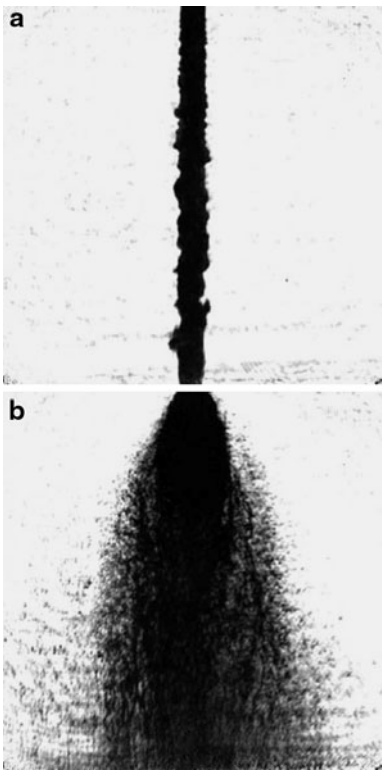

Fig. 16 Ballistic image of flow cases described in Table 2 **a** Case 21: Q_L = 0.98 (L/min), GLR = 0.00; **b** Case 22: Q_L = 0.98 (L/min), GLR = 2.15

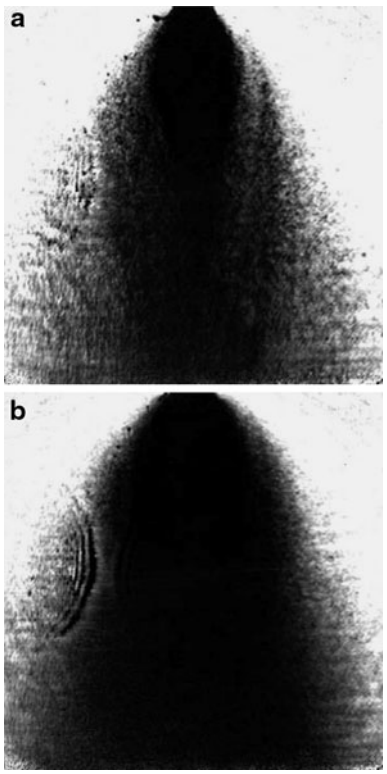

Fig. 17 Ballistic image of flow cases described in Table 2 **a** Case 23: Q_L = 0.98 (L/min), GLR = 4.06; **b** Case 24: Q_L = 0.97 (L/min), GLR = 8.04

increased Q_L and GLR. However, the threshold for this transition changes with nozzle diameter. To first order, this transition appears to obey a power law relating Q_L/D and GLR, as shown in the figure. Hence, at low flow rates, the threshold is nearly independent of GLR, meaning that there is insufficient turbulence or choking to induce rapid atomization even at very high GLR. At intermediate GLR, increased Q_L is critical (for both diameters) to induce a transition to rapid breakup. Finally, at low GLR, the threshold approaches another limit that is nearly independent of Q_L, so that rapid atomization cannot be achieved even at very high Q_L. This analysis provides a possible path forward for predicting when an aerated jet will break up rapidly, although further study is needed to fully characterize the spray behavior for different fuels and nozzle geometries. It seems clear, however, that the breakup of aerated jets is aided in part by increased flow rate due to choking or turbulence in the liquid phase, as well as by GLR.

The evidence also seems to indicate a change in the breakup dynamics even when the jet breaks up rapidly (the solid symbols in Fig. 20). We speculate that the coherent surging and formation of chevrons we observe in many of the motion pictures containing rapid breakup cases is caused by the sudden destruction of large slugs of gas as each of the disks that separate them is burst. Whether or not that really is the case, it is a coherent process that produces wave-like behavior in the droplet field and hence the chevron structures.

It is not possible at this time to define a boundary between the coherent cases (cases that surge coherently and produce chevrons) and the cases that atomize even more rapidly, although we can say that these latter cases occur at the highest value of both Q_L/D and GLR. The instability at this high level of Q_L/D and GLR seems less coherent (more irregular); more like the flapping encountered earlier. We have one 0.5 mm case at GLR = 10 (not included here because it is just one case). It also exhibits incoherent instability. This form of instability could be a shear layer phenomenon (e.g., vortex shedding in the surrounding air), while the surging seems to be a liquid jet phenomenon. A weak shear layer would not produce the very rapid breakup we observe, but it might explain the instability that accompanies it. At the highest level of Q_L/D and GLR, therefore, it seems clear that the very rapid atomization is caused by internal nozzle flows. These more incoherent flows at very high Q_L/D and high GLR produce a wider spray and a more uniform droplet field, which is desirable. In contrast, the surging and collected droplet chevrons would likely enhance thermo-acoustic instabilities in a combustor duct and they are to be avoided.

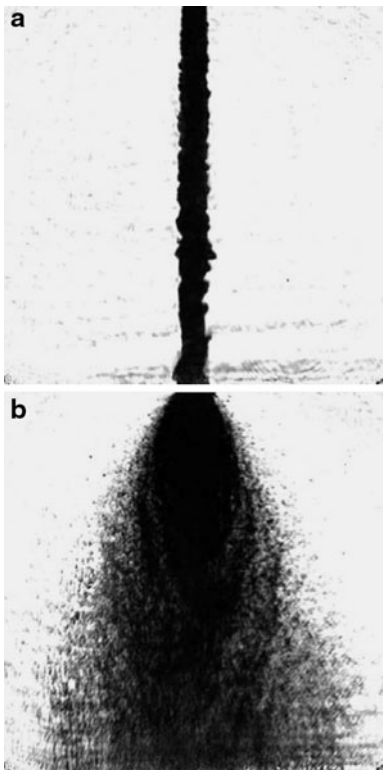

Fig. 18 Ballistic image of flow cases described in Table 2 **a** Case 25: Q_L = 1.11 (L/min), GLR = 0.00; **b** Case 26: Q_L = 1.11 (L/min), GLR = 2.01

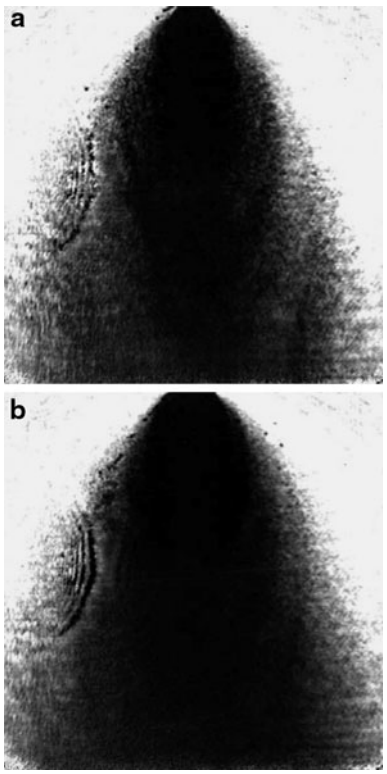

Fig. 19 Ballistic image of flow cases described in Table 2 **a** Case 27: Q_L = 1.13 (L/min), GLR = 4.01; **b** Case 28: Q_L = 1.10 (L/min), GLR = 5.98

It is important to point out that these are simply proposed mechanisms based on observations of ballistic imaging motion pictures and on published flow regime data (e.g., Sovani et al. 2001). What is required is a transmissive nozzle (perhaps the 1 mm device) with observation of the interior flow using a simple optical microscope and high-speed imaging. Ballistic imaging and SLIPI imaging could then be applied to the near-nozzle and overall flow patterns at the same time, to confirm or further elucidate these mechanisms. It would also help to perform particle image velocimetry in the air surrounding the spray to segregate shear layer instabilities from jet core instabilities.

5 Conclusions

The application of ballistic imaging to effervescent jets has revealed important mechanics in the near-nozzle region that have not been observed in prior work. The experimental evidence for two different nozzle sizes indicates that at relatively low flow rates, the jet does not exhibit the wide spread angle and rapid breakup for which effervescent sprays are known. They break up via fairly common mechanisms involving the formation of large ligaments which then break up further into drops, even at very high GLR.

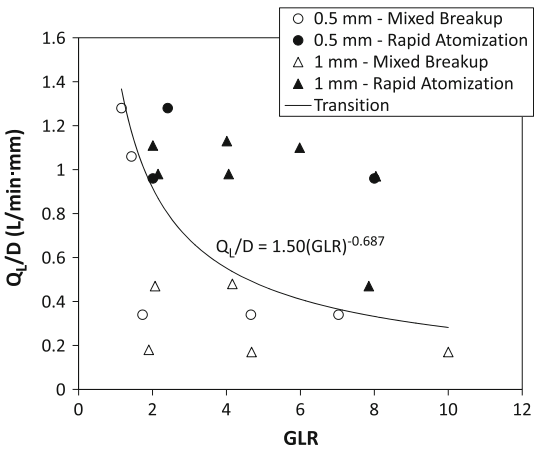

Fig. 20 Regime map for the transition from mixed-mode breakup (*open symbols*) to rapid breakup (*solid symbols*). Both the case of coherent surging leading to formation of chevrons and the more incoherent case leading to even more rapid breakup are represented by the *solid symbols*

At flow rates that exceed this flow rate threshold value, we observe a significant change in the breakup dynamics when the transition from GLR's typical of the bubble-flow regime to GLR's typical of the slug-flow regime occurs. This happens with both nozzle sizes at various total flow rates, and it depends upon the GLR of course. Flows that

have just entered what appears to be the slug-flow regime produce distinct chevrons which are formed by coherent surging. The surging is most likely caused by the sudden destruction of large slugs of gas as each of the disks that separate them is burst. Whatever the source may be, it is a coherent process that produces wave-like behavior in the droplet field and hence the chevron structures. Instability also occurs at higher GLR, but it is less coherent.

These conclusions are based upon entirely new images of the near-nozzle flow, and they are somewhat speculative at this point. Further, simultaneous measurements are required to resolve the remaining questions.

Acknowledgments The authors are grateful for technical assistance from Dr. Shukesh Roy (Spectral Energies, LLC), Mr. Kyle Frische (Innovative Scientific Solutions Inc.), Ms. Amy Lynch (Air Force Research Laboratories), and Dr. K-C. (Stephen) Lin (Taitech Inc.). Dr. Sedarsky was supported by the Swedish Research Council grant no. 621-2004-5504 and Air Force EOARD grant no. FA8655-06-1-3031. Equipment and funding was also provided in part by the Air Force Research Laboratory SBIR program (Barry Kiel, Program Manager) and the Air Force Office of Scientific Research (Drs. Julian Tishkoff and Mitat Birkan, Program Managers).

References

Berrocal E, Kristensson E, Richter M, Linne M, Aldén M (2008) Application of structured illumination for multiple scattering suppression in planar laser imaging of dense sprays. Opt Express 16(22):17,870–17,881

Lee J, Sallam KA, Lin K, Carter C (2009) Spray structure in near-injector region of aerated-liquid jet in subsonic crossflow. J Propuls Power 25(2):258–266

Lefebvre A, Wang X, Martin C (1988) Spray characteristics of aerated-liquid pressure atomizers. J Propuls 4(4):293–298

Lin K, Carter C, Cernucan J, Fezza K, Wang J (2008) Ultrafast X-ray study of aerated-liquid jets in a quiescent environment. In: ILASS Americas, 21st annual conference on liquid atomization and spray systems, Orlando

Lin K, Carter C, Fezza K, Wang J, Liu Z (2009) Multi-zone behavior of transverse liquid jet in high-speed flow. In: Proceedings of the 47th AIAA aerospace sciences meeting, AIAA

Linne MA, Paciaroni M, Berrocal E, Sedarsky D (2009) Ballistic imaging of liquid breakup processes in dense sprays. Proc Combust Inst 32:2147–2161

Paciaroni M (2004) Time-gated ballistic imaging through scattering media with applications to liquid spray combustion. Ph.D. thesis, Division of Engineering, Colorado School of Mines, Golden, CO

Paciaroni M, Linne M (2004) Single-shot two-dimensional ballistic imaging through scattering media. Appl Opt 43:5100–9

Sallam KA, Aalburg C, Faeth GM (2004) Breakup of round nonturbulent liquid jets in gaseous crossflow. AIAA J 42(12): 2529–2540

Sallam KA, Aalburg C, Faeth GM, Lin KC, Carter C, Jackson T (2006) Primary breakup of round aerated-liquid jets in supersonic crossflows. At Sprays 16:657–672

Schmidt J, Schaefer Z, Meyer T, Roy S, Danczyk S, Gord J (2009) Ultrafast time-gated ballistic-photon imaging and shadowgraphy in optically dense rocket sprays. Appl Opt 48(4):B137–B144

Sedarsky D, Gord J, Meyer T, Linne M (2009) Fast-framing ballistic imaging of velocity in an aerated spray. Opt Lett 34(18):2748–2750

Sovani S, Sojka P, Lefebvre A (2001) Effervescent atomization. Prog Energy Combust Sci 27:483–521

Sovani S, Crofts J, Sojka P, Gore J, Eckerle W (2005) Structure and steady-state spray performance of a effervescent diesel injector. Fuel 84:1503–1514